In situ aberration measurement technique based on multi-illumination settings and principal component analysis of aerial images

Dongbo Xu (徐东波)[1,2], Xiangzhao Wang (王向朝)[1*], Yang Bu (步 扬)[1], Lifeng Duan (段立峰)[1,2,3], Guanyong Yan (闫观勇)[1,2], Jishuo Yang (杨济硕)[1,2], and Anatoly Y. Burov[3]

[1] *Laboratory of Information Optics and Opto-Electronic Technology, Shanghai Institute of Optics and Fine Mechanics, Chinese Academy of Sciences, Shanghai 201800, China*

[2] *Graduate University of Chinese Academy of Sciences, Beijing 100049, China*

[3] *Shanghai Mico Electronics Equipment Co., Ltd, Shanghai 201203, China*

[*] *Corresponding author: wxz26267@siom.ac.cn*

Received May 31, 2012; accepted June 20, 2012; posted online October 24, 2012

The impact of lens aberrations becomes severe when the critical dimensions (CDs) shrink. The accurate measurement of both low- and high-order Zernike aberrations is important during a photolithographic process. Based on the multi-illumination settings and principal component analysis of aerial images, a novel *in situ* aberration measurement technique that can accurately measure all the Zernike aberrations, except for the sinusoidal 2-θ and sinusoidal 4-θ terms (under polar coordinates, and Z_1 to Z_4 are not considered) is proposed in this letter. The estimated maximum error of the Zernike aberrations ranges from 0.43 to 0.78 mλ when the amplitudes of the Zernike coefficients range from –20 to 20 mλ. The standard and root mean square errors are both in the range from 0.14 to 0.4 mλ.

OCIS codes: 110.3960, 120.3940, 220.1010.

doi: 10.3788/COL201210.121202.

The critical dimensions (CDs) of integrated circuits have been continuously shrinking for more than two decades. The adverse lithographic impacts of lens aberrations have become increasingly severe. The fast and accurate *in situ* measurement of both low- and high-order Zernike aberrations of lithographic lens is important during the lithographic process. For example, semiconductor manufacturers need such aberration data to simulate processes reliably intended for manufacturing. Therefore, several *in situ* aberration measurement (AM) techniques have been developed to measure the low- and high-order Zernike aberrations rapidly and precisely[1−9]. Duan *et al.*[10,11] have proposed an *in situ* AM technique using aerial images (AIs) based on principal component analysis (PCA) (AMAI-PCA). This technique is fast and accurate, but can only measure low-order astigmatism, spherical, and coma. A novel *in situ* AM technique for lithographic lens using AIs based on PCA and multi-illumination (MI) settings (AMAI-PCAMI) is proposed in this letter based on the work of Duan *et al.*. This technique can measure accurately all the Zernike aberrations, except for the sinusoidal 2-θ terms and 4-θ terms (under polar coordinates), Z_5, Z_7–Z_{12}, Z_{14}–Z_{17}, Z_{19}–Z_{21}, Z_{23}–Z_{28}, Z_{30}–Z_{32}, and Z_{34}–Z_{37} (Z_1–Z_4 are not considered).

The PCA of AI was used by the AMAI-PCA technique to establish a linear regression matrix that links the principal component (PC) coefficients and Zernike coefficients of lens aberrations. The Zernike coefficients can be calculated when the linear regression matrix is established[10]. The accuracy of the Zernike aberration estimation is determined by the linearity between the PC coefficients and Zernike coefficients. A better linearity indicates more accurate measurement results.

Streamlined AI model is linear with respect to Zernike aberrations[12]. Each Zernike aberration that affects the intensity distribution characteristic of an AI should be thoroughly extracted to improve the linearity between the PC coefficients and Zernike coefficients. The AMAI-PCA technique uses conventional illumination setting, in which several Zernike aberrations have similar effects on the intensity distribution of an AI that adversely impacts the linearity between the PC coefficients and Zernike coefficients. Zernike aberration has a different effect on the intensity distribution of an AI when illumination settings are different (Fig. 1). The AMAI-PCAMI technique can thoroughly extract the information on the effects of each Zernike aberration on the intensity distribution of an AI through PCA of AIs under different illumination settings. In addition, the linearity between the PC and Zernike coefficients is improved.

AIs are calculated for each t Zernike combinations designed using the three-dimensional (3D) Box-Behnken design method[13,14]; each AI has a total number of pixels p. The relationship among PCs, PC

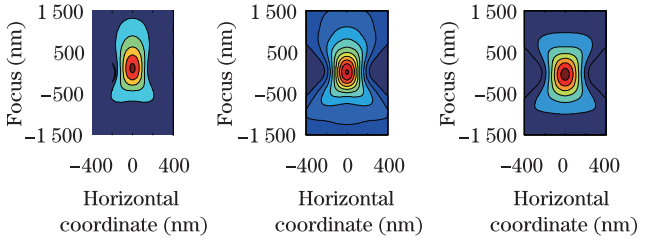

Fig. 1. Effects of Zernike aberration Z_9 on the intensity distribution of AIs under different illumination settings. (a) Conventional σ=0.5, (b) annular $\sigma_{\rm out}$=0.7 and $\sigma_{\rm in}$=0.5, and (c) annular $\sigma_{\rm out}$=0.9 and $\sigma_{\rm in}$=0.7.

coefficients, and AIs is expressed as

$$\mathrm{AIM}^{\sigma_n} = \left[\ \mathrm{PC}_1^{\sigma_n}\ \mathrm{PC}_2^{\sigma_n}, \cdots, \mathrm{PC}_t^{\sigma_n}\ \right] \cdot \begin{bmatrix} V_1^{\sigma_n} \\ V_2^{\sigma_n} \\ \vdots \\ V_3^{\sigma_n} \end{bmatrix} + E_{\mathrm{T}}^{\sigma_n}, \tag{1}$$

where AIM^{σ_n} is the AI matrix, and the images are reshaped into vertical vectors of size $p\times t$; $\mathrm{PC}_i^{\sigma_n}$ is the PC vector of size $p\times 1$, $V_i^{\sigma_n}$ is the corresponding PC coefficient vector of size $1\times t$, and $E_{\mathrm{T}}^{\sigma_n}$ is the residual error of size $p\times t$; σ_n is the partial coherence factor for different illumination settings and subscript 'n' (n= 1,2,3) denotes the illumination setting.

The linear regression matrix between the PC coefficients of AIs and the Zernike coefficients of the lens was established through the linear regression process. The regression matrices are different because of the different illumination settings. The linear regression equation is expressed as

$$\begin{bmatrix} V_1^{\sigma_n} \\ V_2^{\sigma_n} \\ \vdots \\ V_t^{\sigma_n} \end{bmatrix} = \begin{bmatrix} \mathrm{RM}_1^{\sigma_n} \\ \mathrm{RM}_2^{\sigma_n} \\ \vdots \\ \mathrm{RM}_t^{\sigma_n} \end{bmatrix} \cdot \mathrm{ZM} + E_{\mathrm{R}}^{\sigma_n}, \tag{2}$$

where $\mathrm{RM}_i^{\sigma_n}$ is the regression matrix of size $1\times(m+1)$, ZM is the matrix of the Zernike combinations, with the size $(m+1)\times t$, $E_{\mathrm{R}}^{\sigma_n}$ is the residual error of size $t\times t$, and m is the number of Zernike aberrations used to build the model.

The actual AIs in the extraction process are quickly measured under different illumination settings and fitted with PCs corresponding to the same illumination setting to obtain the PC coefficients. This relationship is expressed as

$$\mathrm{AI}^{\sigma_n} = \left[\mathrm{PC}_1^{\sigma_n}\ \mathrm{PC}_2^{\sigma_n}, \cdots, \mathrm{PC}_{qn}^{\sigma_n}\right] \cdot V^{\sigma_n'} + E_{\mathrm{T}}^{\sigma_n'}, \tag{3}$$

where AI^{σ_n} is the actual AI vector of size $p\times 1$, $V^{\sigma_{\mathrm{n}}'}$ is the PC coefficient vector of the actual AI of size $q_n\times 1$, $E_{\mathrm{T}}^{\sigma_{\mathrm{n}}'}$ is the residual error vector of size $p\times 1$, and q_n is the number of PCs used for solving Zernike aberrations.

Zernike aberrations can be solved by

$$\begin{bmatrix} V^{\sigma_1'} \\ V^{\sigma_2'} \\ V^{\sigma_3'} \end{bmatrix} = \begin{bmatrix} \mathrm{RM}^{\sigma_1} \\ \mathrm{RM}^{\sigma_2} \\ \mathrm{RM}^{\sigma_3} \end{bmatrix} \cdot \begin{bmatrix} 1 \\ Z_5 \\ Z_7 \\ Z_8 \\ \cdot \\ Z_{37} \end{bmatrix} + E_{\mathrm{R}}', \tag{4}$$

where $V^{\sigma_1'}$, $V^{\sigma_2'}$, and $V^{\sigma_3'}$ are the PC coefficient vectors of the actual AIs of size $q_n\times 1$; RM^{σ_1}, RM^{σ_2}, and RM^{σ_3} are the regression matrices used to solve the Zernike aberrations of size $q_n\times(1+m)$; E_{R}' is the residual error vector of size $(q_1+q_2+q_3)\times 1$. The PC coefficient matrices $V^{\sigma_n'}$ and regression matrices RM^{σ_n} are given by

$$V^{\sigma_n'} = \begin{bmatrix} V_1^{\sigma_n'} \\ V_2^{\sigma_n'} \\ \vdots \\ V_{q_n}^{\sigma_n'} \end{bmatrix},\ \mathrm{RM}^{\sigma_n} = \begin{bmatrix} \mathrm{RM}_1^{\sigma_n} \\ \mathrm{RM}_2^{\sigma_n} \\ \vdots \\ \mathrm{RM}_{q_n}^{\sigma_n} \end{bmatrix}. \tag{5}$$

The measurement performance of the AMAI-PCAMI was simulated through a standard lithographic simulator tool PROLITHO (KLA-Tencor Co. Ltd.)[15,16]. The linearity between the PC coefficients and Zernike coefficients can be obtained through the linear regression process. The linearity of AMAI-PCAMI was compared with that of AMAI-PCA[10], and an improved linearity has been achieved. The mask pattern and simulation settings for the validation of the comparison results are the same with AMAI-PCA, except for the illumination settings. The AMAI-PCAMI simulation was performed under MI settings. One conventional and two annular illumination settings were used during the simulation. The partial coherence factor σ for the conventional illumination setting was 0.5, whereas the partial coherence factors [σ_{outer}, σ_{inner}] for the annular illumination settings were [0.7, 0.5] and [0.9, 0.7], respectively. The AMAI-PCA measurement was conducted under conventional illumination setting, with partial coherence factor σ of 0.65. The simulation settings are shown by Table 1. The structural pattern of the mask is shown by Fig. 2, which composed of the openings oriented in the 0°/90° direction.

The PCs and PC coefficients were sorted in descending order according to their weight during the PCA process. The linearity between the PC coefficients and Zernike coefficients is established if the linear relationship between them is greater than 0.99. In actual calculation, the first 20 PC coefficients and corresponding linear regression matrices are usually selected. The solving linear equations is constituted with the terms whose linearity between PC and Zernike coefficients is greater than 0.99. Figure 3(a) shows the AMAI-PCAMI linearity, whereas Fig. 3(b) shows the AMAI-PCA linearity.

Figure 3 shows that AMAI-PCAMI has more PC coefficients whose linearity between the Zernike coefficients is greater than 0.99 compared with AMAI-PCA. Therefore, AMAI-PCAMI efficiently improves the linearity between PC coefficients and Zernike coefficients. The rank of the coefficient matrix of solving linear equations (Eq. (4)) is equal to the number of the Zernike aberrations when the low- and high-order Zernike aberrations need calculations. The Zernike aberrations can be calculated through least square fitting. However, only a few terms have a linearity larger than 0.99 if AMAI-PCA is used to solve both the low- and high-order Zernike aberrations. The number of solving linear equations is less than the number of Zernike aberrations that need calculation. Therefore, the aberrations cannot be calculated.

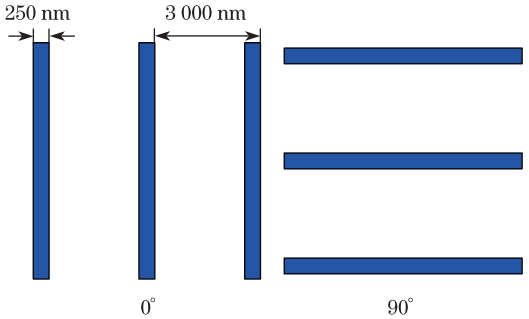

Fig. 2. Structural pattern of the mask used in the simulation for AMAI-PCAMI and AMAI-PCA.

Table 1. Simulation Settings

Parameter	AMAI-PCAMI	AMAI-PCA
Illumination Type, Partial Coherence Factor σ	Conventional: $\sigma = 0.5$ Annular: σ_{outer}=0.7, σ_{inner}=0.5 Annular: $\sigma_{\text{outer}} = 0.9$, σ_{innter}=0.7	Conventional: $\sigma = 0.65$
Wavelength λ (nm)	193	
NA	0.75	
CD (nm)	250	
Pitch (nm)	3 000	
Orientation	0°/90°	
Range of Aerial Image (nm)	X/Y direction: –900–900; Z direction: –3 500–3 500	
Sample Interval (nm)	X/Y direction: 30 Z direction: 125	

A total of 100 groups of normally distributed Zernike aberrations were randomly generated to simulate the aberration distribution in the lithographic lens. PRO LITH was used to simulate the AIs, and Zernike aberrations were solved by AMAI-PCAMI. The absolute deviation between 100 nominal and calculated values of Zernike aberrations was calculated to evaluate the accuracy of AMAI-PCAMI. The calculated accuracy of Zernike aberrations is shown Fig. 4. Max, standard, mean, and RMS errors stand for the maximum,

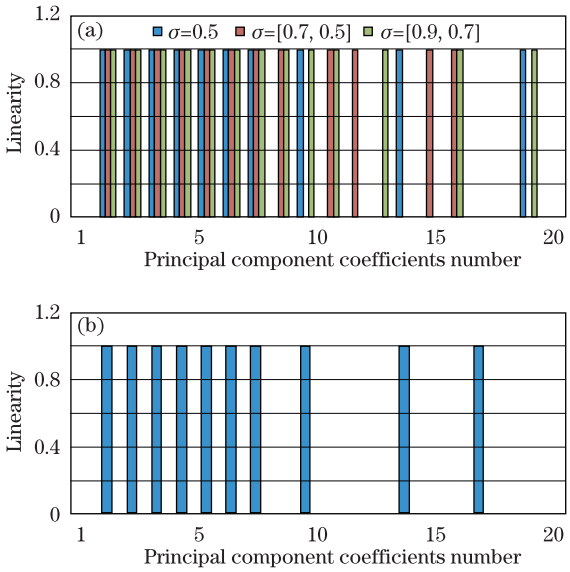

Fig. 3. Linearity between PC and Zernike coefficients. (a) AMAI-PCAMI linearity, and (b) AMAI-PCA linearity.

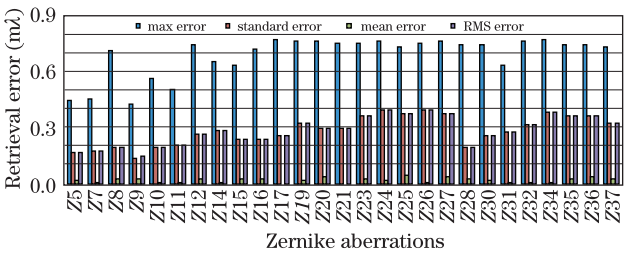

Fig. 4. Zernike aberration simulated measurement accuracy using the AMAI-PCAMI technique, when the amplitude range of Zernike aberrations varies from –20 to 20 mλ.

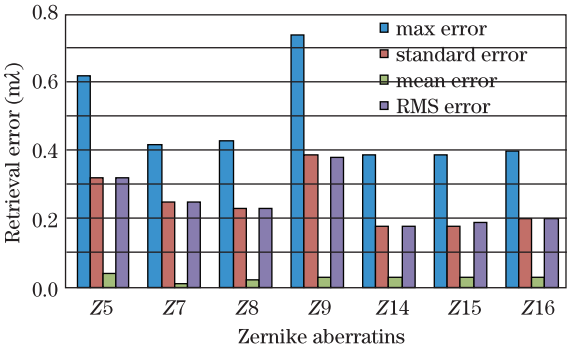

Fig. 5. Zernike aberration simulated measurement accuracy using the AMAI-PCA technique when the amplitude range of Zernike aberrations varies from –20 to 20 mλ.

standard, average, and root mean square errors of 100 deviations, respectively. AMAI-PCAMI can accurately measure all the Zernike aberrations, except for the sinusoidal 2-θ terms and 4-θ terms (under polar coordinates), Z_5, Z_7–Z_{12}, Z_{14}–Z_{17}, Z_{19}–Z_{21}, Z_{23}–Z_{28}, Z_{30}–Z_{32}, and Z_{34}–Z_{37}(Z_1–Z_4 are not considered). The calculated maximum error of Zernike aberrations is from 0.43 to 0.78 mλ. The standard and RMS errors vary within the range from 0.14 to 0.4 mλ.

The accuracy of the Zernike aberrations based on the AMAI-PCA technique is demonstrated in Fig. 5. The accuracy of low-order Zernike aberrations calculated by AMAI-PCA was compared with that by AMAI-PCAMI (Figs. 4 and 5, in which the accuracies of Z_5, Z_7–Z_9, and Z_{14}–Z_{16} were compared). Compared with AMAI-PCA, the average accuracy of the low-order Zernike aberrations solved by AMAI-PCAMI improved by more than 10%.

A novel *in situ* AMAI-PCAMI technique is proposed in this letter. All the Zernike aberrations, except for the sinusoidal 2-θ terms and 4-θ terms (under polar coordinates), Z_5, Z_7–Z_{12}, Z_{14}–Z_{17}, Z_{19}–Z_{21}, Z_{23}–Z_{28}, Z_{30}–Z_{32}, and Z_{34}–Z_{37}(Z_1 to Z_4 are not considered), can be measured accurately using the MI settings and PCA of AIs. The maximum error of Zernike aberrations is from 0.43 to 0.78 mλ when the amplitude range of Zernike coefficients varies from –20 to 20 mλ. The standard and RMS errors are both in the range from 0.14 to 0.4 mλ. Compared with AMAI-PCA, the average accuracy of low-order Zernike aberrations (Z_5, Z_7–Z_9, and Z_{14}–Z_{16}) solved by AMAI-PCAMI improvers by more than 10%.

The AMAI-PCAMI technique exhibits great potential to measure all the 37 Zernike aberrations accurately, with the optimization of the mask and illumination settings.

The authors would like to thank the technical support of the Chinese National Engineering Research Center for Lithographic Equipment. This work was supported by the National Natural Science Foundation of China under Grant No. 60938003.

References

1. J. P. Kirk and C. J. Plogler, Proc. SPIE **3679,** 70 (1999).
2. H. Nomra, K. Tawarayama, and T. Kohno, Proc. SPIE **3679,** 358 (1999).
3. J. P. Kirk, Proc. SPIE **4000,** 2 (2000).
4. J. P. Kirk, G. Kunkel, and A. K. Wong, Proc. SPIE **4346,** 8 (2001).
5. H. Nomra, Proc. SPIE **4346,** 25 (2001).
6. T. Hagiwara, N. Kondo, I. Hiroshi, K. Suzuki, and N. Magome, Proc. SPIE **5754,** 1659 (2005).
7. F. Wang, H. Lu, Q. Zhang, and A. Y. Bourov, Chin. Opt. Lett. (to be published).
8. L. Zavyalova, A. Bourov, and B. W. Smith, Proc. SPIE **5754,** 1728 (2005).
9. W. Liu, S. Liu, T. Zhou, and L. Wang, Opt. Express **17,** 19278 (2009).
10. L. Duan, X. Wang, A. Y. Bourov, B. Peng, and P. Bu, Opt. Express **19,** 18080 (2011).
11. L. Duan, X. Wang, G. Yan, and A. Y. Bourov, Proc. SPIE **8169,** 816909 (2011).
12. A. Y. Bourov, L. Li, Z. Yang, F. Wang, and L. Duan, Proc. SPIE **7640,** 764032 (2010).
13. G. E. P. Box and D. W. Behnken, Technometrics **2,** 455 (1960).
14. T. J. Robinson, *Box–Behnken Designs Encyclopedia of Statistics in Quality and Reliability* (Wiley, New Work, 2008).
15. C. A. Mack, Proc. SPIE **5645,** 63 (2005).
16. C. A. Mack, Proc. SPIE **5754,** 1 (2004).